Sequential vortex hopping in an array of artificial pinning centers

J. C. Keay,[1,*] P. R. Larson,[1] K. L. Hobbs,[1] M. B. Johnson,[1] J. R. Kirtley,[2,3] O. M. Auslaender,[3,4,†] and K. A. Moler[3,4]

[1]*Homer L. Dodge Department of Physics and Astronomy, University of Oklahoma, Norman, Oklahoma 73019, USA*

[2]*IBM Research Division, Yorktown Heights, New York 10598, USA*

[3]*Department of Applied Physics and Geballe Laboratory for Advanced Materials, Stanford University, Stanford, California 94305, USA*

[4]*Stanford Institute for Materials and Energy Science, SLAC National Accelerator Laboratory, Menlo Park, California 94025, USA*

(Received 29 July 2009; revised manuscript received 30 September 2009; published 22 October 2009)

We use low-temperature magnetic force microscopy (MFM) to study the hopping motion of vortices in an array of artificial pinning centers (APCs). The array consists of nanoscale holes etched in a niobium thin film by Ar-ion sputtering through an anodic aluminum-oxide template. Variable-temperature magnetometry shows a transition temperature of 7.1 K and an enhancement of the magnetization up to the third matching field at 5 K. Using MFM with attractive and repulsive tip-vortex interaction, we measure the vortex-pinning strength and investigate the motion of individual vortices in the APC array. The depinning force for individual vortices at low field ranged from 0.7 to 1.2 pN. The motion of individual vortices was found to be reproducible and consistent with movement between adjacent holes in the film. The movements are repeatable but the sequence of hops depends on the scan direction. This asymmetry in the motion indicates nonuniform local pinning, a consequence of array disorder and hole-size variation.

DOI: 10.1103/PhysRevB.80.165421 PACS number(s): 68.37.Rt, 74.78.Db, 74.25.Qt

The behavior of vortices in superconductors is both interesting scientifically and important technologically. Vortex motion is of particular interest because it is a common failure mode of superconductor electronics.[1,2] One approach to control vortex motion has been to create defects in which superconductivity is suppressed. These artificial pinning sites (APCs) (Refs. 3–9) are traps for vortices. In addition to preventing vortex motion, APCs allow us to design the actual positions of pinned vortices. This may become important in future superconductor-based devices.[10,11]

In the past, arrays of APCs (dots[12–14] or antidots[5–7,9]) have been fabricated using e-beam and laser-interferometric lithography, and more recently, Nb-coated anodized aluminum oxide (AAO) films.[15,16] The lithographic techniques produce perfectly ordered arrays of macroscopic dimensions with lattice constants that range from 1000 to 400 nm and have APC diameters down to 150 nm. The Nb-coated AAO structure has a triangular lattice of holes with a lattice spacing of about 100 nm, APC diameters of 50 nm, and well-ordered grains microns in size.[16] These structures show enhancements in properties (conductivity, critical current, and magnetization) at a matching field, H_M, corresponding to one superconducting flux quantum ($\Phi_0 = hc/2e = 2.07 \times 10^{-7}$ G cm^2) per APC ($H_M = \Phi_0/A$, where A is the area of the APC unit cell). Further commensurate effects may also be seen at integer multiples of H_M and its rational fractions. These commensurate effects are most often demonstrated with critical current measurements and magnetization loops[3–7,12–16] but have also been observed in direct imaging.[17]

Direct imaging of vortices and their motion has been demonstrated with a variety of scanned probe techniques,[18–23] as well as electron beam[17] and optical techniques.[24] Optical techniques offer real-time observation of vortex motion with limited resolution and electron-beam techniques have high resolution but require special sample preparation. Scanned probe techniques provide both high spatial resolution and, in some cases, the ability to quantify the pinning forces through direct interaction with the vortices.

In this work, we report a method for fabricating well-ordered arrays of nanoscale APCs in niobium films. The films show enhanced magnetization at the first, second, and third matching fields. For low vortex densities, we investigated the uniformity of the pinning strength as well as the motion of superconducting vortices using low-temperature magnetic force microscopy (MFM). We find the depinning force to be in the range 0.7–1.2 pN at $T = 0.70T_c = 5.0$ K. For attractive tip-vortex interaction, we can reproducibly move individual vortices in repeatable jumps which are consistent with movement between adjacent holes in the Nb film. We also observe local variations in the pinning of a single vortex in the array that manifests as a scan direction dependence of the vortex motion between the APCs.

The AAO-patterned films were fabricated by Ar-ion-beam sputter-etching holes in uniform Nb thin films through AAO templates. The uniform Nb films were sputter deposited in a high-vacuum system with a base pressure of 5×10^{-7} Torr using an unbalanced magnetron source (Torus 2C) operating at 0.15 W/cm^2 dc in an Ar atmosphere of 1.7×10^{-3} Torr. The resulting film thickness was about 75 nm. A 500-nm-thick AAO film with a center-to-center hole spacing of 105 nm and a hole diameter of about 50 nm was placed on the Nb layer. The hole (antidot) array was produced by sputter etching the Nb thin film through the AAO template with a 500 eV Ar-ion beam with a dose of 7×10^{17} ions/cm^2. The AAO was then completely removed from the Nb film by etching in a chromic phosphoric solution at 60 °C for 1 h. The patterned samples were 5×5 mm^2.

The samples were investigated using scanning electron microscopy (SEM), atomic force microscopy (AFM), super-

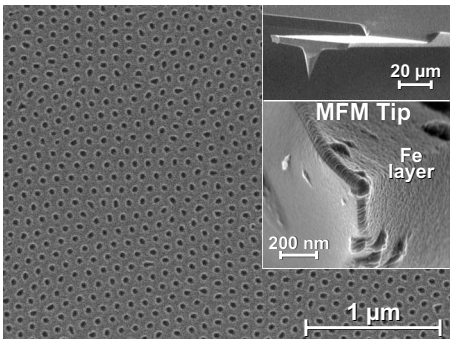

FIG. 1. Plan-view SEM image of the 75-nm-thick Nb nanohole array. Insets are SEM images of the MFM cantilever [MikroMasch (NSC-18/Al)] and probe (top) and MFM probe tip (bottom) used for this work. The probe was coated on one side (right) with about a 60 nm Fe layer extending down from the probe tip.

conducting quantum interference device (SQUID) bulk magnetometry, and MFM. A JEOL 880 SEM was used for plan and cross-sectional investigations. The nanohole array shows a smooth film between well-defined holes and has nanoscale roughness (rms roughness=1.5 nm, excluding holes) typical of sputter-deposited films, as shown in Fig. 1. The white halo around each hole is due to enhanced secondary emission of electrons and not to the presence of a lip, as confirmed by AFM. Magnetization data was acquired with a Quantum Design MPMS XL-7 using a scan length of 25 mm. Comparison of zero-field-cooled temperature scans [see supplemental material (SM) (Ref. 25)] in a 1 Oe field of a uniform 75 nm Nb thin film and nanohole array shows the same transition width as an unprocessed Nb thin film and has a deviation of only 0.2 K of the critical temperature, indicating that the sputter-etched holes have a negligible effect on the film's superconducting properties. MFM was performed using a custom system with a base temperature of about 5 K.[26] The probe was a commercial AFM tip coated by shadow evaporation on one side with a multilayer Ti/Fe/Au coating, with ≈60 nm of Fe, as shown in Fig. 1 inset.

Figure 2(a) shows the magnetization half loops of the 75-nm-thick Nb nanohole array at several temperatures. Clearly the nanohole array produces well-defined steps in the magnetization at matching fields (integer multiples of $H_M \approx 2170$ Oe). At the lowest temperature, 5.0 K ($0.70T_c$), the first two matching-field features are well defined in both directions of the field sweep while the third matching-field feature is strongest on the first quarter of the loop. At $0.84T_c$, the first and second matching-field features are evident before reaching the critical field at ~5000 Oe. At $0.90T_c$, only the first matching-field feature is present before superconductivity is suppressed.

The features in the magnetization half loops at the first matching field correspond to pinning of the vortices in the holes in the Nb film, Fig. 2(a) inset. We calculate that the pinning sites are saturated at this field and higher-order matching-field phenomena occur by vortex pinning at interstitial sites. This follows from estimating the vortex saturation number, n_s, of an APC (Refs. 7, 14, and 27): $n_s = D/[4\xi(T)]$, where D is the APC diameter and $\xi(T) = \xi(0)(1-T/T_c)^{1/2}$ is the temperature-dependent coher-

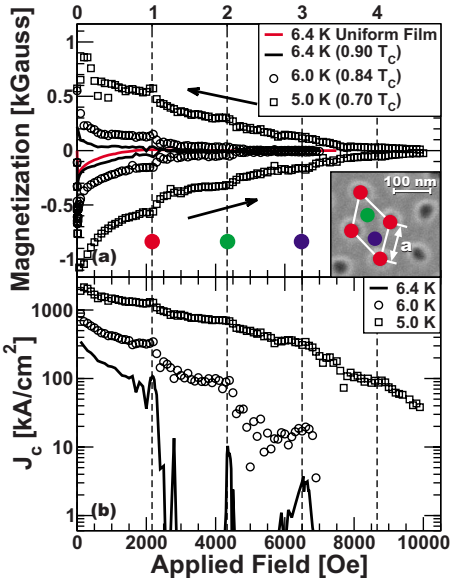

FIG. 2. (Color online) (a) Magnetization half loops, $M(h)$, at different temperatures for the 75-nm-thick Nb nanohole array. The vertical dashed lines mark integer matching fields, $H_M \approx 2170$ Oe. The arrows indicate the direction of the field change. The inset is a plan view SEM image of the nanohole array overlaid with unit cell ($a=105$ nm). The outer red circles indicate vortex positions for the first matching field and the inner green and blue filled circles indicate vortex position for the second and third matching fields. A quarter loop of a uniform 75-nm-thick Nb film at 6.4 K is shown for comparison (red lower line). (b) Estimate of the critical current calculated from the magnetization half loops using the Bean critical-state model for a square thin film of side 5 mm.

ence length of the sample. Using $\xi(0)=13$ nm [from our $H_{c2}(T)$ measurements, in good agreement with others[14,28]] and $D=50$ nm, we find n_s ranges from 0.3 to 0.5 at 0.90 and $0.70T_c$, respectively. At applied fields greater than the first matching field, vortices will be forced to interstitial sites because the antidot sites are saturated.

The fact that we observe a second matching-field feature suggests that pinning is strong enough to stabilize a defective honeycomb lattice, which would otherwise be rendered unstable by vortex-vortex interactions.[8] The interstitial arrangement of the vortex cores is expected to be well ordered and stable at the third matching field.[8] The weaker nature of our observed feature is due to the temperature at which the measurement was acquired. These results are similar to those of Welp *et al.*,[16] who report up to the third matching field for arrays of nanoholes in a Nb film fabricated by directly sputtering Nb on AAO. We find superior superconducting behavior (e.g., higher T_c, narrower transition) of the nanohole films described here (holes etched through AAO in a uniform Nb film) compared with films that we prepared by direct Nb deposition on AAO. However, the conditions of the direct deposition of Nb on AAO were not identical to those for the thin film and nanohole array samples and may account for the observed difference in behavior.

The magnetization in Fig. 2(a) can be used to obtain a rough estimate of the scale of the bulk critical current density, J_c, of the nanohole array. The estimate relies on the

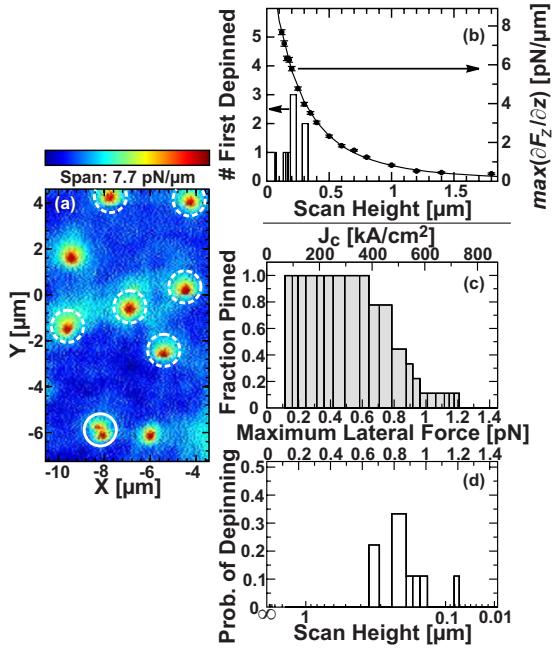

FIG. 3. (Color online) (a) MFM image of the nanohole array cooled to 5 K in the ambient field with tip retracted. The image shows one newly depinned vortex (solid circle), six previously depinned vortices (dashed circle), and two stable vortices (no circle). The tip-sample separation of this scan is 160 nm. The color scale range is 7.7 pN/μm. (b) Number of vortices first depinned at each scan height (left axis) and fitted maximum force gradient (vortex peak height) as a function of tip-sample separation (right axis). (c) The fraction of vortices still pinned as a function of maximum lateral force (lower axis) and critical current density (top axis). (d) Probability of a vortex first depinning as a function of maximum lateral force (upper axis) and tip-sample separation (bottom axis). The critical current density is given by $J_c = \max(F_{\rm lat})/(t\Phi_0)$. The maximum lateral force axis of (c) and (d) are the same.

Bean critical-state model.[29] In this model, the current is assumed to flow uniformly in the thickness of the sample and the vortex configuration is assumed to be critical. With those assumptions and assuming that the sample has cylindrical symmetry $J_c \approx 6\Delta m/(tV)$ (Δm is the magnetic-moment difference of the up and down field sweeps, t is the thickness of the film, and V is the thin-film volume). Figure 2(b) shows that J_c is on the scale of 10^6 A/cm^2 at an applied field of 2 kOe at a temperature of $0.7T_c$.

The vortex-depinning strength can be measured locally using MFM to depin (move) vortices. For this measurement, the sample was cooled from 10 to 5 K in ambient field and a series of images at constant tip-sample distance, z, were acquired with z ranging from 1.80 μm down to 70 nm. Figure 3(a) shows a scan for $z=160$ nm and repulsive tip-vortex interaction. The vortex density, ≈ 0.08 vortices/μm^2, corresponds to a flux density of ≈ 2 G.

Most of the vortices in Fig. 3(a) show a discontinuity during the scan, most apparent in the vortex enclosed by a solid circle. The discontinuity is reminiscent of tip-hop artifacts commonly seen in contact AFM, where it is associated with changes in the AFM tip during a scan. Here we do not see any such tip hops because $z > 50$ nm and the sample surface is very smooth. Instead, the discontinuities are due to vortex motion under the influence of the magnetic MFM tip. At each scan height, forward and reverse scans[30] were acquired and analyzed to determine the maximum z at which any discontinuity appears, corresponding to the first movement of a pinned vortex. In Fig. 3(a), the vortex enclosed by a solid circle first shows movement at this 160 nm high scan, vortices enclosed by dotted circles showed movement in earlier (higher) scans, and, within our experimental sensitivity, two vortices (no outline) have not yet been depinned. Thus, the vortices with either solid or no outlines were more strongly pinned than those with the dotted outlines. Extending this analysis to 21 scans taken for z from 1.80 μm to 70 nm, we can infer the force required to depin vortices. Figure 3(b) shows the number of vortices first depinned at each z (bar graph, left axis). Figure 3(b) also shows the fitted vortex peak heights $[\max(\partial F_z/\partial z)]$ and associated error for each scan height (points, right axis). The solid line is a fit to the theoretical vortex peak height.[25] Note that F_z is the vertical component of the applied force, not the depinning force, which is a lateral force, $F_{\rm lat}$. However, $\max(F_z)$ is related to $\max(F_{\rm lat})$ by a geometrical factor[21] α, in the range 0.3–0.4.[25] For the remainder of this work we use $\max(F_{\rm lat}) = 0.35\ \max(F_z)$. Figures 3(c) and 3(d) combine the data in Fig. 3(b) and show the fraction of vortices which remain pinned at their initial location, Fig. 3(c), and the probability of the first depinning event, Fig. 3(d), as a function of $\max(F_{\rm lat})$ [lower axis Fig. 3(c) and upper axis Fig. 3(d)]. The top axis of Fig. 3(c) shows the critical current density calculated from this $F_{\rm lat}$, $J_c = \max(F_{\rm lat})/(t\Phi_0)$, and the bottom axis of Fig. 3(d) is the corresponding tip-sample separation for $\max(F_{\rm lat})$. Although the critical current is calculated from the onset force, its scale compares well with the rough estimate of the scale that we obtained from the Bean model for the bulk J_c [Fig. 2(b)].[31] As shown in Figs. 3(b)–3(d), the first two vortices depin at $z=300$ nm, corresponding to $\max(F_{\rm lat}) \approx 0.7$ pN; and none remain unperturbed at $z=70$ nm, corresponding to $\max(F_{\rm lat}) \approx 1.2$ pN. Therefore we observe a range of depinning forces from 0.7 to 1.2 pN for our fabricated APC arrays. As expected, these depinning forces are more than an order of magnitude smaller than those calculated using simple models of a vortex interacting with a single pinning site[27,32] because these models do not take into account the attraction of a vortex to adjacent holes. However, using a model that includes an array of holes with similar geometry the depinning force is calculated to be about 3 pN, which is in good agreement with our observed forces.[33]

One can also determine the size and the directions of the vortex jumps from the observed discontinuity and infer that the vortex jumping is consistent with hopping between adjacent holes in the Nb film. For that, we field cooled from 10 to 5 K in a 3 Oe magnetic field with the same polarity as the tip to obtain vortices that are attracted to the tip. In this mode of vortex imaging, the vortex is maintained in the scan field even after a strong perturbation by the tip, allowing long periods of study with many observations of vortex jumps that can be directly correlated with images of the underlying hole structure in the Nb film. Figure 4 shows the forward and reverse scan images of an attractive vortex with a tip-sample

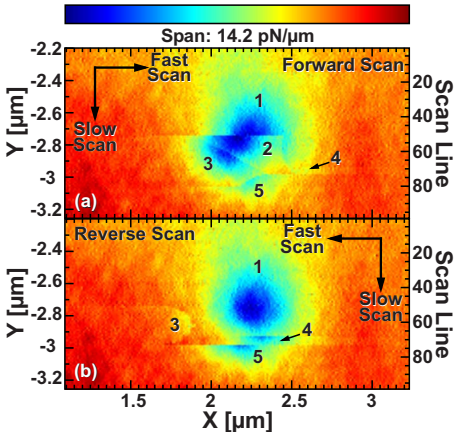

FIG. 4. (Color online) MFM forward and reverse images at 5 K for an attractive tip-vortex interaction with a tip-sample separation of 100 nm. The discontinuities in the images are due to the vortex hopping between five distinct vortex positions. The color scale range is 14.2 pN/μm. The relative positions of the images were corrected for piezohysteresis.

separation of 100 nm. Within these images, we see prominent discontinuities separating five stable vortex positions, labeled 1–5. These discontinuities occur where the tip perturbed the vortex enough to move the vortex from one position to another. The magnitude of the discontinuities is the difference in the measured signal between the initial and final positions of the vortex. Briefly, the vortex maintains position 1 in both the forward and reverse scans for the first 50 scan lines. In the next quarter of the image, the vortex occupies positions 3, 2, and 1 during the forward scans and positions 1 and 3 during the reverse scans. In the following scan lines, the vortex stably occupies positions 3, 2, and 4 in the forward direction, and then 4 and 3 in the reverse direction. The last part of this image shows the vortex hopping between positions 3 and 5 in the forward and reverse scans before stabilizing in position 5 for the remainder of the scan. Below we determine the offset vectors required to "reassemble" the different continuous sections of the scan into a single continuous image of the vortex. The offset vectors correspond to the jumps the vortex made while we imaged it.

To illustrate the "reassembly" process we first analyze the vortex hops between positions 1 and 2. A magnified view of the forward scan image is shown in Fig. 5(a). Dashed and solid white lines overlaid on the image at the discontinuities demark the positions of the tip for each vortex hop. The inset shows an enlarged view of the region where the vortex occupies positions 1 and 2. Close examination of the inset allows us to determine at which pixels the vortex hops. The two horizontal dashed lines indicate the location of the forward scan lines plotted in Fig. 5(b). The black vertical dashed line indicates the position in the image at which the vortex hops from position 2 back to position 1 in the forward scan. From this position to the end of the scan line, the data from the first and second scan lines overlap, as shown in Fig. 5(b). Noting that the vortex image is truncated in the y direction close to the geometric center in both positions, we know that the y component of the hop is much smaller than the x component and can treat hop as if one dimensional

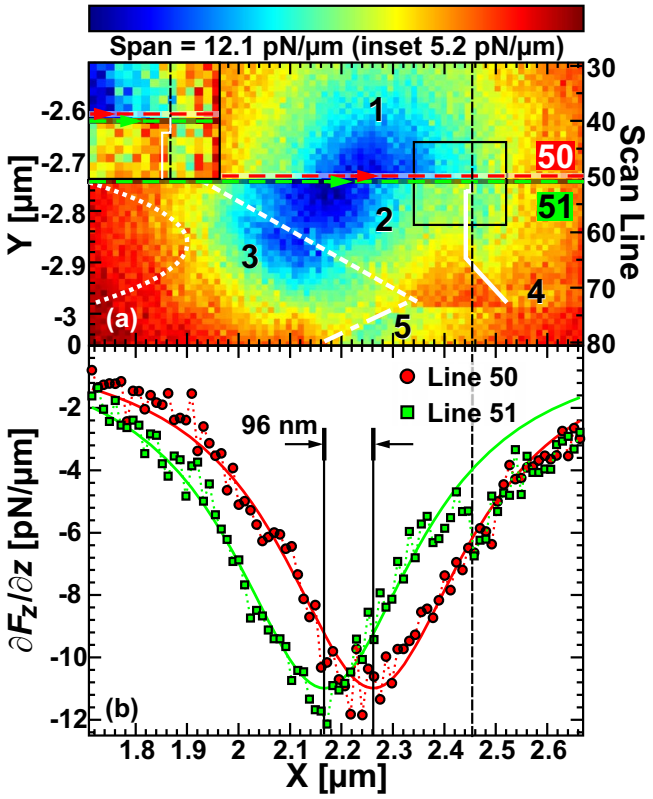

FIG. 5. (Color online) (a) Forward scan image of an attractive vortex-tip interaction (z=100 nm) with metastable vortex-position boundaries highlighted: forward hop between 2 and 1, 4 (white solid), forward hop between 3 and 2 (white dashed), forward hop between 3 and 5 (white dash dot) and reverse hop between 1 and 3 (white dot). The two horizontal dashed lines indicate scan lines used to determine lateral shift of vortex from position 2 to 1. Color scale range is 12.1 pN/μm. The inset shows an enlarged view of the black framed region where the vortex hops from position 2 to position 1. Inset color scale range is 5.2 pN/μm. (b) Line cuts number 50 and 51 from panel (a). Solid circles are data from the unperturbed vortex in position 1. Solid squares are from the following forward scan line, clearly showing the shifted vortex minimum signal at position 2 and the abrupt decrease in $\partial F_z/\partial z$ as the vortex hops from position 2 back to position 1. The solid lines are Lorentzian fits to the data. The error in the fitted positions, ± 6 nm, is shown on the vertical bars which indicate the center positions of the fits. The image was acquired at 5 K.

(1D). The scan lines were fit using a Lorentz function of the form $\partial F_z/\partial z = \gamma/\pi[1/(x-x_0)^2+\gamma^2]$. The scale parameter, γ, and peak position, x_0, were used as fitting parameters to determine γ and x_1 (peak position) for the vortex at position 1, using scan line 50. The scale parameter was fixed for the fitting of the vortex peak position, x_2, at position 2, using scan line 51. By comparing the central position of the two peaks we determine the x component of the vortex hop from position 1 to 2 to be $\Delta x_{1\to 2}=96\pm 8$ nm, in good agreement with the nominal nearest-neighbor distance. The section of the image containing the vortex at position 2 was then translated in the $+x$ direction by $\Delta x_{1\to 2}$ and overlaid on the section of the reverse scan image containing the vortex at position 1. The vortex is almost completely imaged at position 1 in the reverse scan direction [Fig. 4(b)]. The variance (aver-

age squared difference) of the overlapping pixels between the translated vortex section and the reverse scan image of the vortex at position 1 was used to quantify the quality of fit. In the other vortex hops, the x and y components are comparable and the vortex image does not necessarily contain the central minimum. This decreases the reliability of 1D and two-dimensional (2D) fitting of the vortex at these positions. Instead, we allow each section (bounded by the discontinuities) of the forward and reverse scan images containing a single vortex position to freely move over the reverse scan image of the vortex at position 1 and minimize the variance. The resulting shift gives the location of the vortex at each position relative to vortex position 1. We performed this calculation using bootstrapping[34] and find an estimated error of about 10 nm in x and y for the vortex positions. The positions of the vortex are then determined by a 2D monopole-monopole fit[21,23,25] of the "full" vortex at position 1. The results of the vortex-position fitting including associated errors are shown in Fig. 6(a). The vortex positions are shown superimposed on the MFM image of the nearly continuous vortex (from the reverse scan). Also shown are the measured positions of the nearby holes in the niobium film. The 50 nm holes are shown as solid open circles along with surrounding dashed circles representing the error in the hole (APC) positions. The positions of the APCs were determined from three subsequent scans with tip-sample separations of 80 and two at 60 nm.[25] The hole positions taken from these scans had standard deviations of 10 nm (~1 pixel). This error was random and not systematic from sources such as drift of the sample or creep of the piezoelectric scanner. The positions of the vortex were translated together about 80 nm (Ref. 25) to minimize the distance between the vortex positions and the APCs. We do this because it is well known that the magnetic (vortices) and topographic (APCs) images may not be aligned[35] and tip asymmetry is not considered in this simple model.[25] Moreover, it is more energetically favorable for the vortex to be positioned in the APC than located interstitially in the nanohole array. Agreement is good, especially considering that the circulating currents around the core decay on the scale of $\lambda_{\mathrm{eff}} \approx 300$ nm.[36] The sequence and repeat count of the tip-induced vortex hopping is summarized in Figs. 6(b) and 6(c). The sequence ends with the vortex stable at position 5. We found this hopping to be repeatable, reproducible, and controllable within the nanohole array as the hopping sequences described above were observed in another scan at the same scan height.

The interaction between the magnetic tip and the vortex can be better understood by considering their relative positions just before hopping. These were determined from the distinct boundaries observed in Figs. 4 and 5. The hopping behavior is displayed in the SM (Ref. 25) as a movie of the tip scanning across the film surface synchronized with the position of the vortex. Also included in this movie is a solid circle of radius $r_{\mathrm{max}}=550$ nm around the tip representing the approximate position of maximum lateral force from the tip.[25] The movie shows that a vortex hops in the direction that the tip moves, typically when the *trailing* edge of the circle of maximum lateral force moves over the vortex. The polar plot of Fig. 6(d) gives the radial distance and angle from the initial (solid) and final (open) vortex positions to

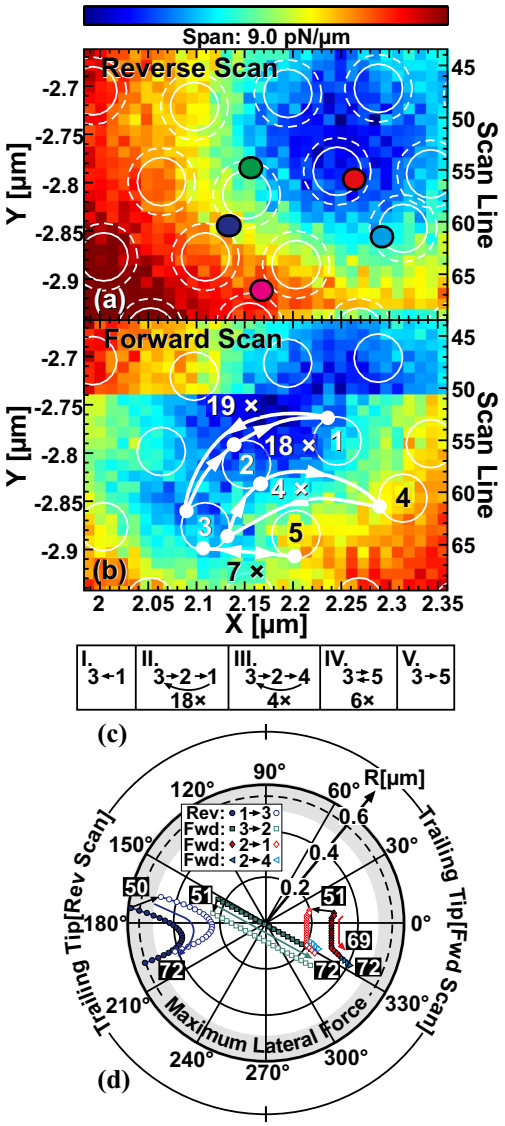

FIG. 6. (Color online) (a) Reverse scan image with $z=100$ nm. The filled circles indicate the estimated vortex positions and their size the associated error. The solid white circles show the positions and nominal diameter of the APCs while the white dashed circles indicate the associated errors in the positions of the APCs. (b) Forward scan image with $z=100$ nm showing the enumerated vortex positions, hopping directions, and number of repeats of the hopping cycle. The white circles highlight the locations of the APCs. Color scale range is 9.0 pN/μm for both images. (c) Table of depinning events showing the direction of the vortex movement and the number of repeats in the cycle. (d) Polar plot illustrating the distribution of the depinning events measured from the vortex to the MFM tip before (solid) and after (open) a depinning event. The gray ring indicates the region, 0.55 ± 0.06 μm, of maximum lateral force between the vortex and the MFM tip. Initial and final scan line numbers of an event group are displayed at top and bottom of a symbol group. The images were acquired at 5 K.

the tip for each hopping event. The dashed line indicates the radius of maximum lateral force between the vortex and the tip. The shapes of the locus of the points for these hops are the same as the dotted, dashed, and solid boundaries, respectively, in Fig. 5(a). The hop from position 1 to 3 and the hop

from 2 back to 1 are closely associated with the passing of the trailing edge of the maximum force curve while the intermediate hop from 3 to 2 is associated with the passing of the tip itself.

It is not surprising for a vortex to hop when the lagging edge of the circle of maximum lateral force passes over it. It is, however, surprising that we do not see a similar hop with the leading edge or, in fact, that the vortex does not follow the tip, hopping from APC to APC, but rather, only jumps between a few sites. The vortex following the tip would be expected if the sample were uniform, with perfectly ordered and identically sized holes. Such an array would produce a flat, uniform vortex-film energy surface with ordered, deep minima (due to the holes) and a vortex would move regularly under the influence of the tip. However, the sample is not uniform, the ordering is not perfect and the shape and size of the holes vary (see Fig. 1). These nonuniformities result in long-range variations in the vortex-film energy surface. The fact that the vortex only hops between a few sites or holes suggests that these holes are in a shallow minimum. This is supported by the fact that the vortex was initially in this region after the sample was field cooled. Moreover, the vortex always returned to the same initial position between scans.

Another interesting feature of the vortex hopping is the inherent repeatability, but the lack of reversibility, observed in the hopping sequences. This is most clear in the hopping sequences summarized in Fig. 6(c). Here, on the reverse scan, the vortex hops from positions 1 to 3, 19 times and returns via 3 to 2 to 1, 18 times. First, it is reasonable that in hopping from 1 to 3 the vortex must pass through position 2 but it is not found to remain in this position long enough for the slow MFM imaging to capture it there (each line scan takes a few seconds). Still, the dynamics of the reverse and forward hopping sequences are very different. In fact, as shown in Fig. 6(c), the hop from 3 to 2 observed in the forward direction is atypical because it tends to occur when the tip is over the vortex itself. The lack of reversibility may have a contribution from the magnetic asymmetry of tip (see Fig. 1, inset). Although the tip asymmetry is weak (cf. near-radial symmetry of stationary vortices in, e.g., Fig. 4, reverse scan), given the complexity of the tip-vortex interaction and the vortex behavior, some difference between a forward scan and a reverse scan is not surprising. As previously described, defects in the APC lattice may also contribute to the lack of reversibility. For example, the observed APC positions and calculated vortex positions, Fig. 6(a), give a smaller spacing between positions 2 and 3 than from positions 1 to 2 and may contribute to the observed behavior. A model that incorporates both the tip asymmetry and the lattice defects may explain the data.

In this work, we report a method for fabricating well-ordered arrays of nanoscale APCs in niobium films. The films show enhanced magnetization at the first, second, and third matching fields. For low vortex densities, we investigated the uniformity of the pinning strength as well as the motion of superconducting vortices using low-temperature MFM. We find the depinning force to be in the range 0.7–1.2 pN at $T=0.70T_c=5.0$ K. For attractive tip-vortex interactions, we can reproducibly move individual vortices in repeatable jumps consistent with motion between adjacent holes in the Nb film. Although the movement is reproducible and repeatable, the vortices are preferentially trapped in specific pinning sites. This trapping behavior may be attributed to the disorder in the array and variations in APCs. In addition, the vortex motion is not symmetric with respect to the scan direction. This may be a further manifestation of the APC array inhomogeneities or a hint that tip asymmetry may play a role.

We gratefully acknowledge useful discussions with H. Fertig and D. Priour. We thank D. B. Brunski for creating the supplementary material video. Work at the University of Oklahoma was supported by NSF under Grants No. DMR-0080054 and No. NSF-0132534. Work at Stanford was supported by the U.S. Air Force Office of Scientific Research under Contract No. FA50-05-1-0290. This work was also supported by the Center for Probing the Nanoscale (CPN), an NSF NSEC, NSF Grant No. PHY-0425897 and the Department of Energy, Office of Basic Energy Sciences, Division of Materials Sciences and Engineering, under Contract No. DE-AC02-76SF00515.

*Corresponding author; keay@nhn.ou.edu

†Present address: Department of Physics, Technion–Israel Institute of Technology, Haifa 32000, Israel.

[1] P. Selders and R. Wördenweber, Appl. Phys. Lett. **76**, 3277 (2000).

[2] T. J. Shaw, John Clarke, R. B. van Dover, L. F. Schneemeyer, and A. E. White, Phys. Rev. B **54**, 15411 (1996).

[3] D. D. Morrison and R. M. Rose, Phys. Rev. Lett. **25**, 356 (1970).

[4] O. Daldini, P. Martinoli, J. L. Olsen, and G. Berner, Phys. Rev. Lett. **32**, 218 (1974).

[5] A. T. Fiory, A. F. Hebard, and S. Somekh, Appl. Phys. Lett. **32**, 73 (1978).

[6] V. Metlushko, M. Baert, R. Jonckheere, V. Moshchalkov, and Y. Bruynseraede, Solid State Commun. **91**, 331 (1994).

[7] V. V. Moshchalkov, M. Baert, V. V. Metlushko, E. Rosseel, M. J. Van Bael, K. Temst, Y. Bruynseraede, and R. Jonckheere, Phys. Rev. B **57**, 3615 (1998).

[8] C. Reichhardt, C. J. Olson, and F. Nori, Phys. Rev. B **57**, 7937 (1998).

[9] Z. Jiang, D. A. Dikin, V. Chandrasekhar, V. V. Metlushko, and V. V. Moshchalkov, Appl. Phys. Lett. **84**, 5371 (2004).

[10] C. Weeks, G. Rosenberg, B. Seradjeh, and M. Franz, Nat. Phys. **3**, 796 (2007).

[11] M. Berciu, T. G. Rappoport, and B. Jankó, Nature (London) **435**, 71 (2005).

[12] J. I. Martín, M. Vélez, A. Hoffmann, I. K. Schuller, and J. L. Vicent, Phys. Rev. B **62**, 9110 (2000).

[13] J. I. Martín, M. Vélez, J. Nogués, and I. K. Schuller, Phys. Rev.

Lett. **79**, 1929 (1997).
[14] A. Hoffmann, P. Prieto, and I. K. Schuller, Phys. Rev. B **61**, 6958 (2000).
[15] U. Welp, Z. L. Xiao, J. S. Jiang, V. K. Vlasko-Vlasov, S. D. Bader, G. W. Crabtree, J. Liang, H. Chik, and J. M. Xu, Phys. Rev. B **66**, 212507 (2002).
[16] U. Welp, Z. L. Xiao, V. Novosad, and V. K. Vlasko-Vlasov, Phys. Rev. B **71**, 014505 (2005).
[17] K. Harada, O. Kamimura, H. Kasai, T. Matsuda, A. Tonomura, and V. V. Moshchalkov, Science **274**, 1167 (1996).
[18] H. F. Hess, R. B. Robinson, R. C. Dynes, J. M. Valles, and J. V. Waszczak, Phys. Rev. Lett. **62**, 214 (1989).
[19] J. R. Kirtley, M. B. Ketchen, K. G. Stawiasz, J. Z. Sun, W. J. Gallagher, S. H. Blanton, and S. J. Wind, Appl. Phys. Lett. **66**, 1138 (1995).
[20] M. Roseman and P. Grütter, Appl. Surf. Sci. **188**, 416 (2002).
[21] E. W. J. Straver, J. E. Hoffman, O. M. Auslaender, D. Rugar, and K. A. Moler, Appl. Phys. Lett. **93**, 172514 (2008).
[22] O. M. Auslaender, L. Luan, E. W. J. Straver, J. E. Hoffman, N. C. Koshnick, E. Zeldov, D. A. Bonn, R. Liang, W. N. Hardy, and K. A. Moler, Nat. Phys. **5**, 35 (2009).
[23] L. Luan, O. M. Auslaender, D. A. Bonn, R. Liang, W. N. Hardy, and K. A. Moler, Phys. Rev. B **79**, 214530 (2009).
[24] P. Goa, H. Hauglin, M. Baziljevich, E. Il'yashenko, P. Gammel, and T. Johansen, Supercond. Sci. Technol. **14**, 729 (2001).
[25] See EPAPS Document No. E-PRBMDO-80-051940 for magnetometry transition temperature measurements, calculations used for the vortex peak height fitting, determination of the APC positions and a movie illustrating the vortex hopping during imaging. For more information on EPAPS, see http://www.aip.org/pubservs/epaps.html.
[26] E. W. J. Straver, Ph.D. thesis, Stanford University, 2004.
[27] G. S. Mkrtchyan and V. V. Shmidt, Sov. Phys. JETP **34**, 195 (1972).
[28] V. G. Prokhorov, Low Temp. Phys. **24**, 410 (1998).
[29] M. Däumling and D. C. Larbalestier, Phys. Rev. B **40**, 9350 (1989).
[30] A forward scan image is comprised of scan lines acquired with the MFM tip traveling in the $+x$ direction and reverse scan image is comprised of scan lines acquired in the $-x$ direction. Each scan line is acquired with a constant y position with the reverse scan line retracing the forward scan line.
[31] At low magnetic field one expects the bulk critical current to correspond to a force larger than the onset force. The onset force gives an estimate of the local pinning forces while the bulk critical current gives an estimate of the strongest pinning sites in the sample.
[32] T. L. Hylton and M. R. Beasley, Phys. Rev. B **41**, 11669 (1990).
[33] D. J. Priour and H. A. Fertig, Phys. Rev. B **67**, 054504 (2003); and private communications.
[34] B. Efron and R. Tibshirani, 1st ed., *An Introduction to the Bootstrap* (Chapman and Hall, London/CRC, Cleveland, 1994).
[35] A. Volodin, K. Temst, C. V. Haesendonck, Y. Bruynseraede, M. I. Montero, and I. K. Schuller, Europhys. Lett. **58**, 582 (2002).
[36] A. I. Gubin, K. S. Il'in, S. A. Vitusevich, M. Siegel, and N. Klein, Phys. Rev. B **72**, 064503 (2005).